PERFORMANCE MEASURES OF A ROBOTIC MICROPOSITIONER

JAMES D. LEE, JAMES S. ALBUS, NICHOLAS G. DAGALAKIS
and TSUNGMING TSAI
Robot Systems Division, National Bureau of Standards,
Gaithersburg, MD 20899

ABSTRACT

This work describes a computer simulation of the dynamics and control of a robotic micropositioner. The robotic micropositioner is a parallel link manipulator which has six actuators, each controlled independently by a hydraulic system. The dynamic equations of the micropositioner are derived. The control algorithm for path tracing is formulated and tested. In this work the performance of the micropositioner is investigated as function of damping, speed, payload, and location of target.

INTRODUCTION

Most of today's industrial robots are constructed from a series of rigid elements connected by means of rotational joints. Control forces are applied to these joints to position the end-effector. In contrast to this configuration, the actuators/links assembled in the parallel link manipulator are not staged one atop the other; rather, each link serves a role equal to its neighbors. The robotic micropositioner studied in this work is a parallel link manipulator. It can be used as a robot manipulator by itself or as a robot wrist by attaching it to a robot arm.

The idea of parallel link manipulator was first used for the design of flight simulators by Stewart [1]. Studies have been conducted for its use as a mechanical wrist [2], a compliant device for inserting a peg in a hole [3], a force/moment or position sensor [4], and a robot arm [5-11]. Recently, the Robot System Division at NBS has built, analyzed, and measured the stiffness of six-cable robot crane suspension system [12-13]. Lee et al [14] proposed a new design of a parallel link manipulator, rigorously derived the dynamic equations of the system, formulated and through computer simulation tested the control algorithms for position control, path tracing, and force control. In this work, attention is focused on the performance measures of the robotic micropositioner in path tracing.

DESIGN

The front view and the top view of the parallel link manipulator and its coordinate systems are shown in Fig. 1. The manipulator consists of (1) a lower platform which is fixed in space, (2) an upper platform which is movable with respect to the lower platform, and (3) six actuators which link the two platforms together. The (x, y, z) coordinate system is fixed in space with the origin located at the center of the lower platform and the z-axis is normal to the lower platform. The (α, β, γ) coordinate system is embeded in the upper platform. The origin of the (α, β, γ) coordinate system is the center of the upper platform to which the γ-axis is normal. At reference state, the two platforms are parallel,

the orientation of the space (x, y, z) axes coincides with that of the body (α, β, γ) axes, and the distance between the two platforms is denoted by h.

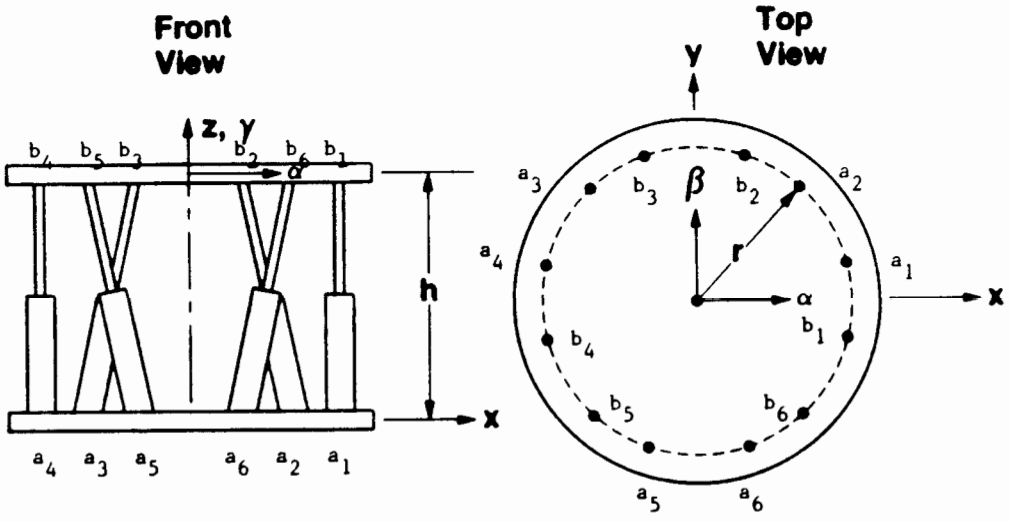

Fig.1 The Parallel Link Manipulator, in its Reference State, and the Coordinate Systems

The i-th piston (i = 1,2,3,...,6) is pinned at point a_i, on the lower platform, and point b_i, on the upper platform. The coordinates of a_i and b_i are

$$a_i: \quad (x_i, y_i, z_i) = (r \cos \Gamma_i, r \sin \Gamma_i, 0), \tag{1}$$

$$b_i: \quad (\alpha_i, \beta_i, \gamma_i) = (r \cos \Delta_i, r \sin \Delta_i, 0), \tag{2}$$

where

$$(\Gamma_1, \Gamma_2, \Gamma_3, \Gamma_4, \Gamma_5, \Gamma_6) = (10^\circ, 50^\circ, 130^\circ, 170^\circ, 250^\circ, 290^\circ), \tag{3}$$

$$(\Delta_1, \Delta_2, \Delta_3, \Delta_4, \Delta_5, \Delta_6) = (-10^\circ, 70^\circ, 110^\circ, 190^\circ, 230^\circ, 310^\circ) \tag{4}$$

An end-effector may be attached to the upper platform and, in this work, the end-effector is considered a pin of length L_p and normal to the upper platform. The coordinate of the tip of the pin is $(0, 0, L_p)$ in the (α, β, γ) coordinate system.

In this work, the actuators are six identical pistons, each controlled independently by a hydraulic system. The piston and its control system is schematically shown in Fig. 2. The governing equation for the piston has been obtained as [14] :

$$f = -d_1\beta^*\dot{l} + d_2p^\circ\left\{\frac{A_2\eta^\circ + A_3\delta^\circ}{A_2\eta^\circ + A_3\delta + d_2(l-l^\circ)} - \frac{L+C-l^\circ}{L+C-l}\right\}, \tag{5}$$

where f is the piston force; l is the piston length; δ (the height of the third chamber) is the control variable; β^* is the damping coefficient which characterizes the orifice V; C is a constant, equal to the difference between the piston

length, l, and the height of the fourth chamber, ξ; p_j and A_j (j = 1,2,3,...,5) are the pressure and the effective cross-section area of the j-th chamber, respectively. A variable with a superscript o indicates the numerical value of that variable at the reference state, and

$$d_1 \equiv A_4^2 \quad , \quad d_2 \equiv A_2 A_4 / A_5 \quad . \tag{6}$$

Eqn. (5) can be symbolically written as

$$f = f\,(\,l\,,\dot{l}\,,\delta\,) \quad , \tag{7}$$

which means the piston acts like a viscoelastic solid whose force-length relation can be controlled by changing the control variable, δ. Moreover, the damping coefficient can be adjusted by changing the orifice cross-section area [15]. The stiffness can be adjusted by changing p^o (the value of p_2 and p_3 at the reference state). Since the six pistons and their hydraulic control systems are identical, eqn.(5) is the general governing equation for all six pistons.

It is assumed that the piston forces and the piston lengths of the six pistons are measurable. In this work, only the ideal situation is considered -- no "noise" of any kind has been introduced into the sensors or the controllers. In other words, no error is involved with the measurements of piston forces and piston lengths, and the servo mechanism can accurately set the control variables as commanded.

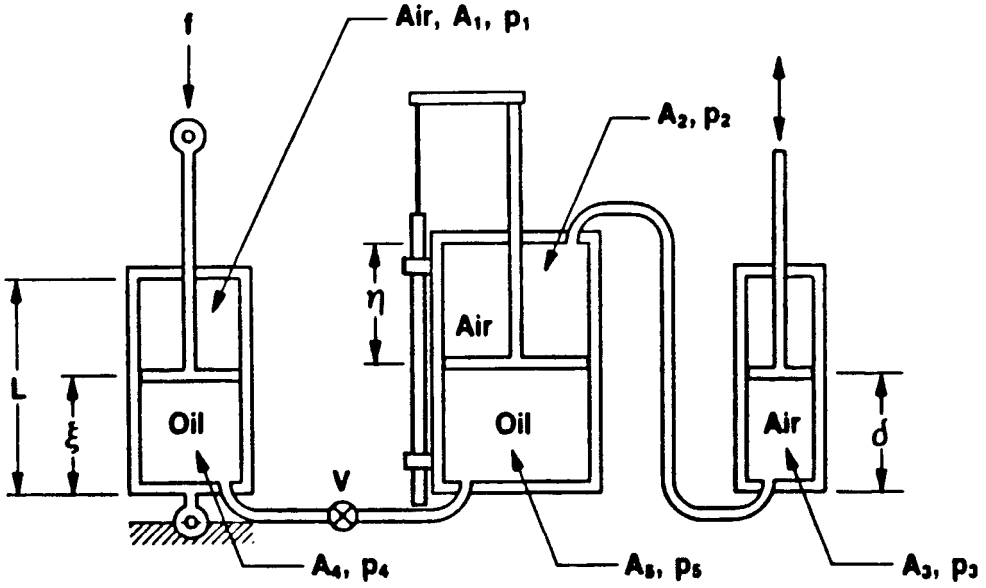

Fig.2 The Schematic Diagram of the Hydraulic Control System of the Piston

DYNAMIC EQUATIONS

Let u_x, u_y, u_z be the displacement components of the center of the upper platform. The rigid body rotation of the upper platform is defined by three succesive (Eulerian) angles of rotation : the sequence starts with rotating the upper platform by an angle ϕ about the γ-axis, followed by an angle θ about the

α-axis and, finally, by an angle ψ about the β-axis. Then the space coordinates of a generic point on the upper platform, after it is rotated and displaced, may be obtained as

$$\begin{bmatrix} x \\ y \\ z \end{bmatrix} = \mathbf{P} \begin{bmatrix} \alpha \\ \beta \\ \gamma \end{bmatrix} + \begin{bmatrix} u_x \\ u_y \\ u_z + h \end{bmatrix}, \tag{8}$$

where the transformation matrix, $\mathbf{P}$, can be expressed as

$$\mathbf{P} = \begin{bmatrix} \cos\psi\cos\phi - \sin\psi\sin\theta\sin\phi & -\cos\theta\sin\phi & \sin\psi\cos\phi + \cos\psi\sin\theta\sin\phi \\ \cos\psi\sin\phi + \sin\psi\sin\theta\cos\phi & \cos\theta\cos\phi & \sin\psi\sin\phi - \cos\psi\sin\theta\cos\phi \\ -\sin\psi\cos\theta & \sin\theta & \cos\psi\cos\theta \end{bmatrix}. \tag{9}$$

The angular velocity, $\boldsymbol{\omega}$, may be written as

$$\omega_\alpha = \dot{\theta}\cos\psi - \dot{\phi}\sin\theta\sin\psi , \tag{10}$$

$$\omega_\beta = \dot{\psi} + \dot{\phi}\sin\theta , \tag{11}$$

$$\omega_\gamma = \dot{\theta}\sin\psi + \dot{\phi}\cos\theta\cos\psi , \tag{12}$$

The dynamic equations for the upper platform have been derived to be [14] :

$$M\ddot{u}_x = F_x , \tag{13}$$

$$M\ddot{u}_y = F_y , \tag{14}$$

$$M\ddot{u}_z = F_z , \tag{15}$$

$$\begin{aligned} &\dot{A}_\theta - (I_{\alpha\alpha}\omega_\alpha + I_{\alpha\beta}\omega_\beta + I_{\alpha\gamma}\omega_\gamma) \dot{\phi}\sin\theta\sin\psi \\ &\quad - (I_{\beta\alpha}\omega_\alpha + I_{\beta\beta}\omega_\beta + I_{\beta\gamma}\omega_\gamma) \dot{\phi}\cos\theta \\ &\quad + (I_{\alpha\gamma}\omega_\alpha + I_{\beta\gamma}\omega_\beta + I_{\gamma\gamma}\omega_\gamma) \dot{\phi}\sin\theta\cos\psi \\ &\quad = M_\theta , \end{aligned} \tag{16}$$

$$\begin{aligned} &\dot{A}_\psi + (I_{\alpha\alpha}\omega_\alpha + I_{\alpha\beta}\omega_\beta + I_{\alpha\gamma}\omega_\gamma) \omega_\gamma \\ &\quad - (I_{\alpha\gamma}\omega_\alpha + I_{\beta\gamma}\omega_\beta + I_{\gamma\gamma}\omega_\gamma) \omega_\alpha \\ &\quad = M_\psi , \end{aligned} \tag{17}$$

$$\dot{A}_\phi = M_\phi , \tag{18}$$

where

$$\begin{aligned} A_\theta \equiv\ &(I_{\alpha\alpha}\omega_\alpha + I_{\alpha\beta}\omega_\beta + I_{\alpha\gamma}\omega_\gamma) \cos\psi \\ &+ (I_{\alpha\gamma}\omega_\alpha + I_{\beta\gamma}\omega_\beta + I_{\gamma\gamma}\omega_\gamma) \sin\psi , \end{aligned} \tag{19}$$

$$A_\psi \equiv I_{\alpha\beta}\omega_\alpha + I_{\beta\beta}\omega_\beta + I_{\beta\gamma}\omega_\gamma , \tag{20}$$

$$\begin{aligned} A_\phi \equiv\ &- (I_{\alpha\alpha}\omega_\alpha + I_{\alpha\beta}\omega_\beta + I_{\alpha\gamma}\omega_\gamma) \cos\theta\sin\psi \\ &+ (I_{\alpha\beta}\omega_\alpha + I_{\beta\beta}\omega_\beta + I_{\beta\gamma}\omega_\gamma) \sin\theta \\ &+ (I_{\alpha\gamma}\omega_\alpha + I_{\beta\gamma}\omega_\beta + I_{\gamma\gamma}\omega_\gamma) \cos\theta\cos\psi . \end{aligned} \tag{21}$$

M_θ , M_ψ , and M_ϕ are moments about the line of nodes, the body y-axis, and the space z-axis, respectively, while the line of nodes is defined to be the body x-axis before the rotation ψ takes place. In terms of the moments about the space axes, M_θ , M_ψ , and M_ϕ can be expressed as

$$M_\theta = M_x \cos\phi + M_y \sin\phi \quad , \tag{22}$$

$$M_\psi = -M_x \sin\phi\cos\theta + M_y \cos\phi\cos\theta + M_z \sin\theta \quad , \tag{23}$$

$$M_\phi = M_z \quad . \tag{24}$$

In Eqns.(13-21), M and $\mathbf{I}$ are the mass and the (mass) moment of inertia tensor of the upper platform, respectively. The generalized forces defined as

$$\mathbf{F} = (F_x, F_y, F_z, M_x, M_y, M_z)^T \tag{25}$$

may be divided into two parts : (1) those due to the piston forces, $\mathbf{F}_p$, and (2) the externally applied forces and moments (including those due to gravity), $\mathbf{F}_a$, i.e.,

$$\mathbf{F} = \mathbf{F}_p + \mathbf{F}_a \quad . \tag{26}$$

PATH TRACING

One of the basic tasks for a robot to perform is for its end-effector to trace a specified curve in space within a given time. In this work, the task is for the pin to trace an n-sided polygon of which the vertices are located at (x_k, y_k, z_k) $(k = 1,2,3,....n)$. The tip of the pin has to travel from (x_k, y_k, z_k) to $(x_{k+1}, y_{k+1}, z_{k+1})$ in a given time interval T_k. The polygon is assumed to be properly contained in the work space of the robotic micropositioner.

At time t^*, where

$$t^i(k) \equiv \sum_{m=1}^{k-1} T_m \;\le\; t^* \;\le\; t^f(k) \equiv \sum_{m=1}^{k} T_m \quad , \tag{27}$$

the tip of the pin should reach

$$\begin{aligned} x^* &= x_k + [t^* - t^i(k)](x_{k+1} - x_k)/[t^f(k) - t^i(k)] \quad , \\ y^* &= y_k + [t^* - t^i(k)](y_{k+1} - y_k)/[t^f(k) - t^i(k)] \quad , \\ z^* &= z_k + [t^* - t^i(k)](z_{k+1} - z_k)/[t^f(k) - t^i(k)] \quad . \end{aligned} \tag{28}$$

where $t^i(1)=0$ and, $(x_{n+1}, y_{n+1}, z_{n+1}) = (x_1, y_1, z_1)$. The generalized coordinates, $\mathbf{q}$, defined as

$$\mathbf{q} \equiv (u_x, u_y, u_z, \theta, \psi, \phi) \quad , \tag{29}$$

are chosen to be $\mathbf{q}^*$ at $t=t^*$, where

$$\begin{aligned} & u_x^* = 0 \;\; , \;\; u_y^* = 0 \;\; , \;\; \phi^* = 0 \;\; , \\ & u_z^* = z^* - h - \sqrt{L_p^2 - x^{*2} - y^{*2}} \quad , \\ & \psi^* = \sin^{-1}(x^*/L_p) \quad , \\ & \theta^* = -\sin^{-1}[y^*/(L_p \cos\psi^*)] \quad . \end{aligned} \tag{30}$$

There is redundancy involved in the task of path tracing because the micropositioner has six degrees of freedom and a curve in space is only three

dimensional. Also, the rotation about the axis of the pin does not affect the path traced by the pin. The use of generalized coordinates as, for example, $\mathbf{q}^*$ in eqns.(30) is one of many ways to eliminate the redundancy.

The mapping from the generalized coordinates to the piston lengths,

$$\mathbf{L} \equiv (l_1, l_2, l_3, \ldots l_6) = \mathbf{G}^{-1}(\mathbf{q}) \quad , \tag{31}$$

is referred to as "inverse kinematics", and the mapping from the piston forces, $\mathbf{f} \equiv (f_1, f_2, \ldots f_6)$, to its resultant forces and moments, $\mathbf{F}$, at the specific generalized coordinates,

$$\mathbf{F} = \mathbf{H}(\mathbf{f}, \mathbf{q}) \quad , \tag{32}$$

is referred to as "forward-force kinematics". Therefore, inverse-force kinematics may be represented as

$$\mathbf{f} = \mathbf{H}^{-1}(\mathbf{F}, \mathbf{q}) \quad . \tag{33}$$

Now, the piston lengths and the piston forces at $t=t^*$ can be calculated as

$$\mathbf{L}^* = \mathbf{G}^{-1}(\mathbf{q}^*) \quad , \tag{34}$$

$$\mathbf{f}^* = \mathbf{H}^{-1}(-\mathbf{F}_a, \mathbf{q}^*) \quad . \tag{35}$$

Then the control variable, $\delta_i^*(i=1,2,\ldots 6)$, can be obtained as

$$\delta_i^* = \frac{R\eta^\circ + \delta^\circ}{f_i^*/f^\circ + [(L+C-l^\circ)/(L+C-l_i^*)]} - R\eta^\circ - f^\circ(l_i^*-l^\circ)/A_3 p^\circ \quad , \tag{36}$$

where

$$R \equiv A_2/A_3 \quad , \qquad f^\circ \equiv p^\circ A_2 A_4/A_5 \quad .$$

Because iterative procedures are required for the solution of eqn.(35), it is proposed to calculate the control variables at discrete times : T, $T+\Delta t$, $T+2\Delta t$, ... $T+m\Delta t$. The control variables at any time t, $t_1 \le t \le t_2$, can be interpolated as

$$\delta(t) = \delta(t_1) + \frac{t-t_1}{t_2-t_1}\delta(t_2) \quad , \tag{37}$$

where t_1 and t_2 are two succesive discrete times at which the control variables, $\delta(t_1)$ and $\delta(t_2)$, are calculated.

PERFORMANCE MEASURES

The control algorithm described above has been tested through computer simulation. The ability of the robotic micropositioner to trace a path can be measured as follows : First, the difference between the desired position, (x^*, y^*, z^*) from eqns.(28), and the actual (simulated) postition, (x', y', z'), at $t = t^*$, can be calculated as

$$e(t^*) = \left\{(x^*-x')^2+(y^*-y')^2+(z^*-z')^2\right\}^{1/2} \quad . \tag{38}$$

For the time interval $[t_i, t_f]$, the index of performance measure, I, is defined as

$$I \equiv \frac{1}{(t_f-t_i)C_l}\int_{t_i}^{t_f} e(t)dt \quad , \tag{39}$$

where C_l is the characteristic length of the curve in space to be traced and, for

an n-sided polygon, C_l is considered to be the sum of the edge lengths which bound the polygon, i.e.,

$$C_l = \sum_{k=1}^{n} [(x_{k+1}-x_k)^2+(y_{k+1}-y_k)^2+(z_{k+1}-z_k)^2]^{1/2} \quad . \tag{40}$$

For illustrative purpose, consider that the polygon to be traced is a square which can be expressed as :

$$(x_1, y_1, z_1) = (2, 1, 9) \quad , \quad (x_2, y_2, z_2) = (2, 2, 9) \quad ,$$
$$(x_3, y_3, z_3) = (1, 2, 9) \quad , \quad (x_4, y_4, z_4) = (1, 1, 9) \quad . \tag{41}$$

The unit of length used in this work is the inch. The given time intervals are $T_k = 2$ seconds (k=1,2,3,4). The applied generalized forces , F_a, are zeroes. The numerical values of all parameters used in this paper, unless otherwise stated, are the same as those in Ref. [14]. It is found that the performance of the micropositioner is a function of the damping coefficient, β^*, and the index of performance measure is at a minimum, $I=I_o$=0.0001591, when the damping coefficient is around $\beta_o = 0.6$. For this standard case described above, the computer simulated results (the dots) and the desired path (the solid lines) are plotted in Fig.3. It is seen that the error (the difference between the desired path and the simulated path) is negligible to the naked eye. This is consistent with that the index of performance measure, I (=0.0001591), is a very small value.

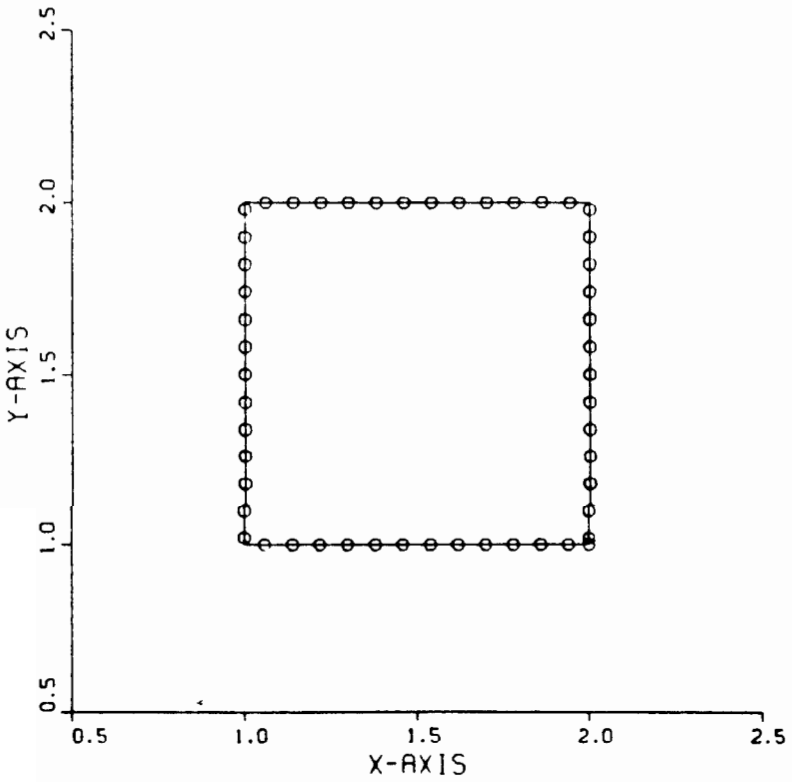

Fig.3 Path Traced in the Standard Case
$T_k = 2$ *sec.* ; $F_a = 0$;
$\beta^* = 0.6$; $I = 0.0001590$

Now keep $\beta^* = \beta_0$; $\mathbf{F}_a = 0$; and the location of the target (the square) at the same place as indicated in eqns.(41); change the time intervals $T_k (k=1,2,3,4)$ to be 0.4 second and 4 seconds in two separate cases. It is not suprising to find that I increases to 0.002588 for $T_k = 0.4$ second and decreases to 0.00006434 for $T_k = 4$ seconds. This means that the robotic micropositioner performs better if it is allowed to trace the path at a slower speed.

For the next case, keep the location of the target, the damping coefficient, and the time intervals to be the same as those in the standard case and change the applied generalized forces to be

$$\mathbf{F}_a = (2.0, 2.0, 2.0, 2.0, 2.0, 2.0) \quad . \tag{42}$$

The index of performance measure changes only slightly to 0.0001935 and the results are plotted in Fig.4. This indicates that the robotic wrist works equally well under externally applied loading provided the robot has *a priori* knowledge of the loading.

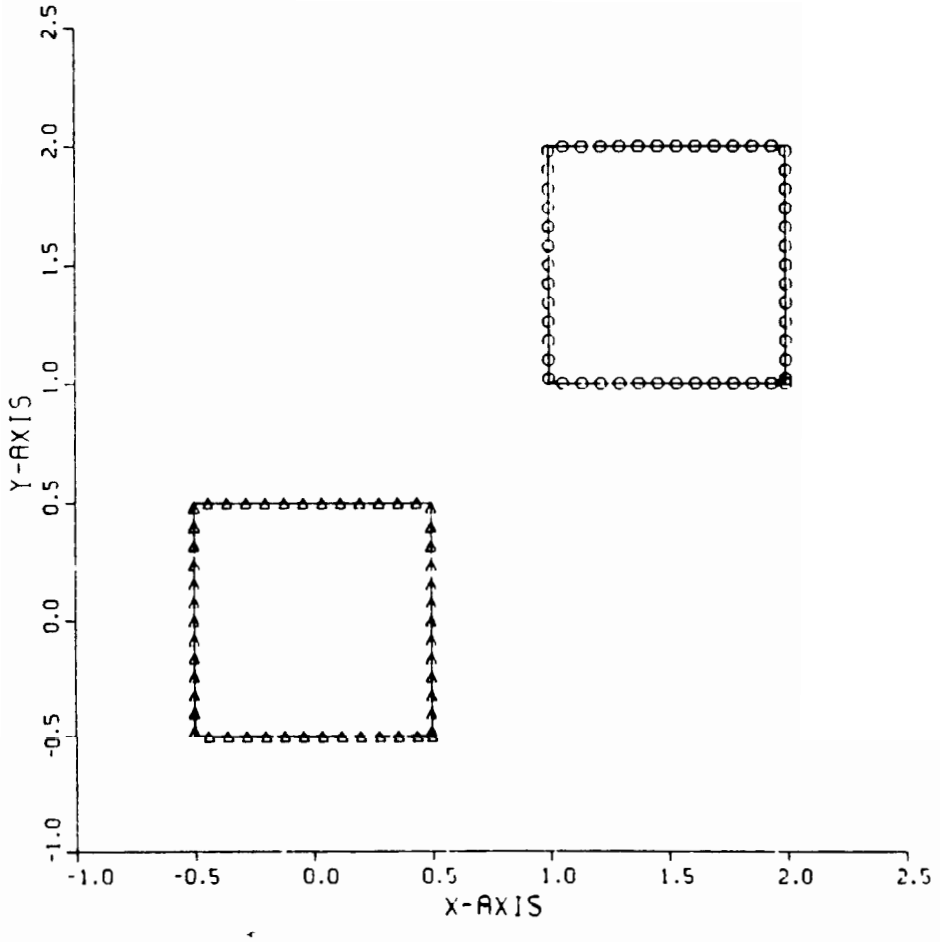

Fig. 4 Paths Traced (1) Under Applied Loading, F_a = (2, 2, 2, 2, 2, 2) , and (2) at Central Location.

Finally, change the location of the target to

$$(x_1, y_1, z_1) = (0.5, -0.5, 9) \quad , \quad (x_2, y_2, z_2) = (0.5, 0.5, 9) \quad ,$$
$$(x_3, y_3, z_3) = (-0.5, 0.5, 9) \quad , \quad (x_4, y_4, z_4) = (-0.5, 0.5, 9) \quad , \qquad (43)$$

and keep all the other parameters to be the same as those in the standard case. In this case, the index of performance measure changes only slightly to 0.0002283; the computer simulated results are also plotted in Fig. 4. In general, the performance of a robot to trace a curve in space depends on the location of the target. It is indeed quite encouraging to see that the change from Fig. 3 to Fig. 4 is minimal. This means the robotic micropositioner, with the proposed control algorithm, performs quite uniformly within its work space.

REFERENCES

1. Stewart, D., "A Plateform with Six Degrees of Freedom", Proc. of the Inst. of Mech. Eng., Vol. 180, Part I, No. 15 pp.371-386, 1965-1966.
2. Bennett, W. M., "Mechanical Wrist for a Robot Arm", Mech. Eng. Dept., Mass. Inst. of Tech., B.S. Thesis, 1968.
3. McCallion, H., Johnson, G. R., Pham, D. T., "A Compliant Device for Inserting a Peg in a Hole", The Industrial Robot, pp.81-87, June 1979.
4. Koliskor, A. S., "Development and Investigation of Industrial Robots Based on Specification by l-coordinates", Soviet Engineering Research, Vol.2, No.12, pp.75-78, 1982.
5. Fichter, E. F., McDowell, E. D., "A Novel Design for a Robot Arm", Proc. Int. Computer Tech. Conf., pp. 250-256, Aug. 1980, San Francisco, California.
6. Fichter, E. F., "Kinematics of a Parallel Connection Manipulator", ASME Paper 84-DET-45 delivered at the Design Eng. Tech. Conf., Oct. 1984, Cambridge, Massachusetts.
7. Fichter, E. F., "A Stewart Platform Based Manipulator: General Theory and Practical Construction", The Kinematics of Robot Manipulators, MIT Press, pp.165-190, 1987.
8. Powell, I. L., "The Kinematic Analysis and Simulation of the Parallel Topology Manipulator", The Marconi Review, Vol.XLV, No.226, pp.121-138, 3rd quarter 1982.
9. Landsberger, S. E., Sheridan, T. B., "A New Design for Parallel Link Manipulators", Proc. Systems Man and Cybernetics Conf., pp.812-814, Nov.1985, Tuscon, Arizona.
10. Sheridan, T. B., "Human Supervisory Control of Robot Systems", Proc. Int. Conf. on Robotics and Automation, pp.808-812, Apr. 1986, San Francisco, California.
11. Konstantinov, M. S., Sotirov, Z. M., Zamanov, V. B., Nenchev, D. N., "Force Feedback Control of Parallel Topology Manipulating Systems", Proc. 15th Int. Symp. on Industrial Robots, pp.181-188, Sep.1985, Tokyo, Japan.
12. Dagalakis, N. G., Albus, J. S., Wang, B. L., Unger, J., Lee, J. D., "Stiffness Study of a Parallel Link Robot Crane for Shipbuilding Applications", Proc. of the 7th Int. Conf. on Offshore Mechanics and Arctic Engineering, pp.29-37, February, 1988, Houston, Texas.
13. Albus, J. S., Dagalakis, N. G., Wang, B. L., Unger, J., Lee, J. D., Yancey, C. W., "Available Robotics Technology for Applications in Heavy industry", Iron and Steel Engineer Magazine (in press).

14. Lee, J. D., Albus, J. S., Dagalakis, N. G., and Tsai, T., "Computer Simulation of a Parallel Link Manipulator", Robotics and Computer-Integrated Manufacturing, to be published.
15. Ogata, K., System Dynamics, Prentice-Hall, Inc., Englewood Cliffs, New Jersey, 1978.